EPR Studies of Tb^{4+} in Single Crystals of Zircon and Scheelite Structure Silicates and Germanates

S. Hansen, B. D. Mosel, W. Müller-Warmuth, and P. E. Fielding[a]

Institut für Physikalische Chemie der Westfälischen Wilhelms-Universität, Schlossplatz 4/7, D-48149 Münster

[a] The University of New England, The Geophysical Research Institute, Armidale, NSW 2351, Australia

Z. Naturforsch. **51a**, 885–894 (1996); received May 14, 1996

In memoriam Professor Gerhard Lehmann

Electron paramagnetic resonance spectra of tetravalent terbium ions have been observed in host crystals of $ZrSiO_4$, $HfSiO_4$, $ThSiO_4$, $ThGeO_4$ (zircon structure) and $ZrGeO_4$, $HfGeO_4$ (scheelite structure) at X band and Q band and various temperatures. The spin Hamiltonian parameters have been determined from the rotational diagrams; the zero field splittings turned out to be extremely large, so that complex spectra far from the strong magnetic field limit had to be analyzed. In all the compounds Tb^{4+} substitutes for the tetragonal metal lattice sites. The incorporation of terbium, the origin of the large second-order parameters and comparisons with the spectra of trivalent gadolinium in similar systems are discussed.

1. Introduction

Electron paramagnetic resonance (EPR) studies of rare earth transition group ions in host cystals with tetragonal structure have already attracted considerable interest. Materials with zircon structure or the closely related scheelite structure profit from their thermal and chemical stability and may be easily doped with a number of different rare earth ions. The use of such materials in solid state lasers or phosphor matrices has provided only a part of the motivation for the EPR studies. More important is the application of high spin S-state ions in host crystals, such as Eu^{2+}, Gd^{3+} and Tb^{4+}, as ideal probes of crystalline electric fields.

Tb^{4+} has the configuration $4f^7$ and possesses an $^8S_{7/2}$ ground state. First examinations of zircon doped with Tb^{4+} [1, 2] point to the occurrence of large zero field splittings (ZFS); more systematic investigations on various zircons and scheelites were thought to be useful in addition to concurrent studies of Gd^{3+}. Tetravalent terbium in its anomalous valence state is of course less stable; it can be recognized in contrast to Tb^{3+} by its colour. Hyperfine structures may arise from the $I = 3/2$ nuclear spin of ^{159}Tb. There are rather few EPR studies so far. In addition to those already mentioned, EPR of Tb^{4+} in cubic ThO_2 [3, 4] and CeO_2 [5, 6] was reported and furthermore in CaF_2 [7, 8]. More recent work deals with $BaTbO_3$ [9, 10], $SrTbO_3$ [9], and $SrMgF_4$ [11].

In the present research, single crystals of the silicates $MSiO_4$ and germanates $MGeO_4$ with M = Zr, Hf, Th were grown, and a small percentage of Tb_4O_7 was added to the melt. The systems with Zr and Hf appeared to be coloured, those with Th were colourless and had to be oxidized by X irradiation.

Reprint requests to Prof. W. Müller-Warmuth.

2. Experimental Procedures

2.1 Crystal Growth

Crystals of $ZrSiO_4$, $HfSiO_4$, $ThSiO_4$ were grown from the flux system $Li_2O + 3MoO_3$; this has been reported elsewhere [12]. The Tb_2O_3 was 99,9% pure as received and was further purified by repeated precipitation of the oxalate and calcination to the oxide; all other reagents were analytical grade or better. Minor variations in soaking time and temperature and of the cooling rate were used to optimize crystal size. The above flux system did not yield suitable crystals of $ThGeO_4$, $ZrGeO_4$ and $HfGeO_4$. In this case the flux system, $PbO + PbF_2 + MoO_3$, described by Wanklyn [13] was used; the growth conditions were similar to those outlined in this reference. It should be noted that this flux composition will produce only monoclinic $ThSiO_4$, whereas the alkali molybdate flux system produces the tetragonal form.

0932-0784 / 96 / 0800-0885 $ 06.00 © – Verlag der Zeitschrift für Naturforschung, D-72072 Tübingen

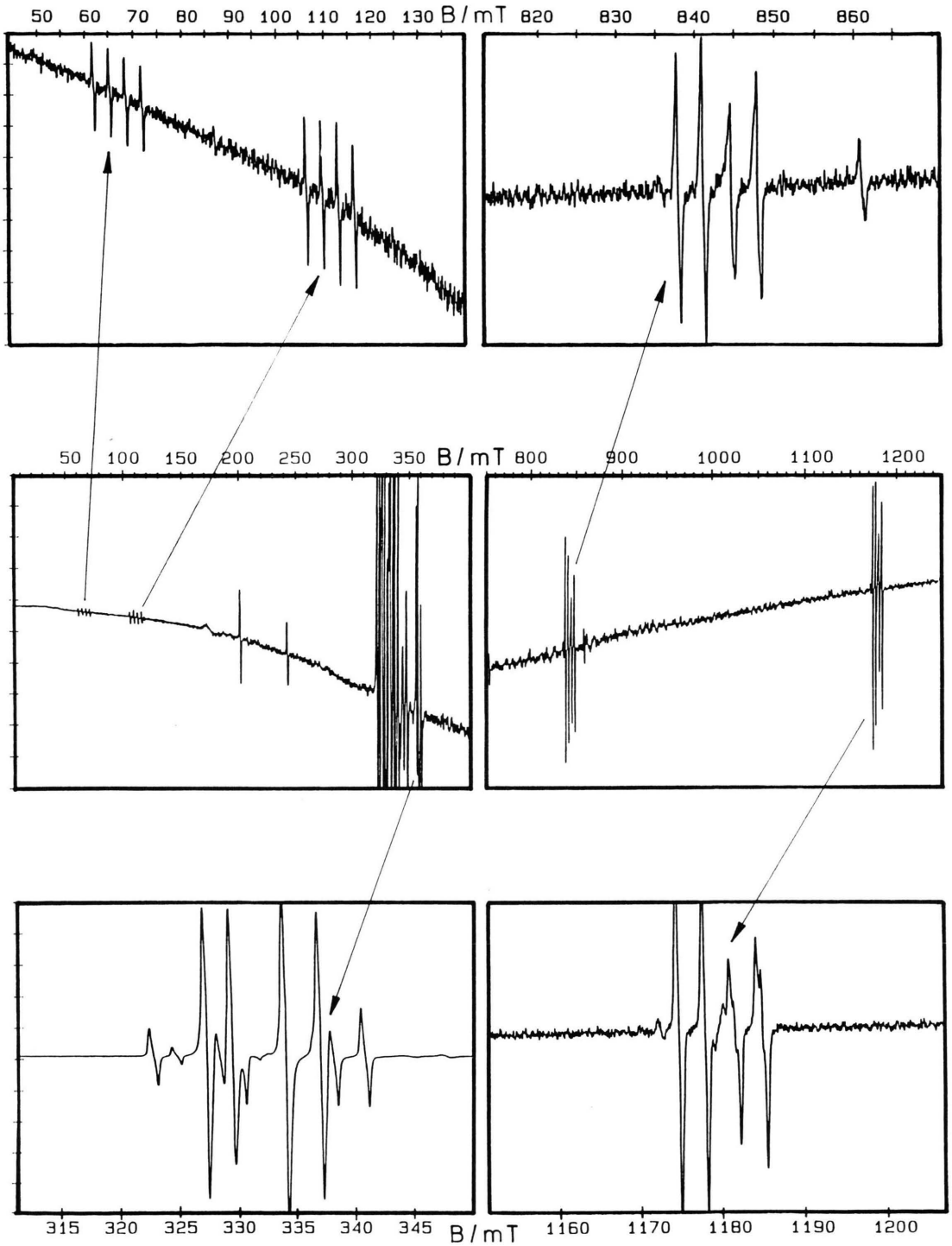

Fig. 1. EPR spectra of Tb^{4+} in $ZrSiO_4$:Tb^{4+} with $B_0 \parallel c$ measured at 9.379 GHz and 77 K. Centre: complete spectrum in the sweep ranges 0 ... 400 mT and 800 ... 1200 mT. Top and bottom: interesting features of the spectrum in an expended scale.

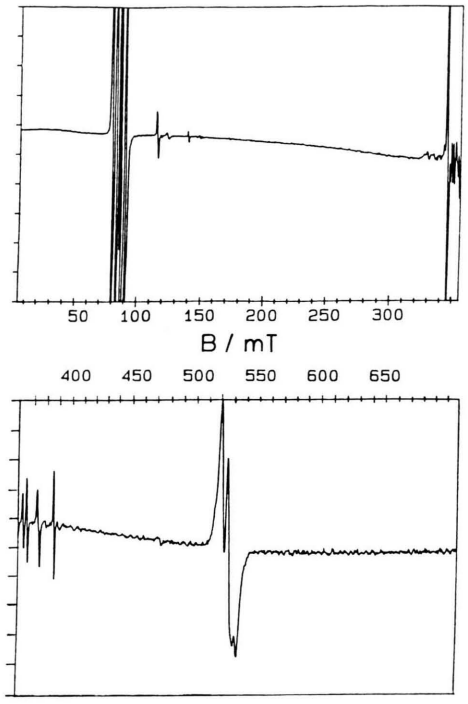

Fig. 2. Same as Fig. 1, but with $B_0 \perp c$, and without expanded details.

2.2 EPR Spectroscopy

The EPR measurements were made on conventional Bruker spectrometers at Q-band (Type B-ER 420 Q) and X-band frequencies (ESP 300). Some of the single crystals were that small that only Q-band data could be recorded. Both spectrometers were equipped with appropriate refrigeration systems and NMR gaussmeters. Data were taken at 293 K and 77 K, in some cases in addition at 50 K. The microware frequency was determined using piceine ($g = 2.00141(1)$) as standard.

The single crystal samples were mounted in the respective cavity and could be rotated about axes according to the morphology of the crystal. All the crystals studied had the same tetragonal bipyramidal habit, and the EPR line positions were first measured at orientations with the crystallographic c axis parallel and perpendicular to the magnetic field. Figures 1 and 2 show an example. Slight misorientations could be corrected in the course of the fitting procedure. It was then necessary to rotate the crystals in steps of 2° about these axes. The result are rotational diagrams of the type of Figure 3. The procedure was computer driven and fully automated. For this and the whole detection of the EPR spectra home-made programs were available [14].

2.3 Data Analysis

The spectra were manipulated using home-made programs for the search of peaks, construction and fitting of rotational diagrams and simulation [14, 15]. The fitting program included a matrix diagonalization followed by a least-squares fit of the field positions for the two rotations with the principal g values, the zero field splitting (ZFS) parameters, B_n^m, the positions of the principal axes in the crystallographic system and the orientation of the crystal in the laboratory system (misorientation).

The data were described by the spin Hamiltonian [16]

$$\hat{\mathrm{H}} = \mu_{\mathrm{B}} \hat{\boldsymbol{S}} \mathbf{g} \boldsymbol{B} + \sum_{n=2}^{2S} \sum_{m=-n}^{n} B_n^m \hat{\mathrm{O}}_n^m + \hat{\boldsymbol{S}} \mathbf{A} \hat{\boldsymbol{I}} \qquad (1)$$

with the Stevens operators $\hat{\mathrm{O}}_n^m$ [17] and the ZFS parameters B_n^m to be determined ($m \leq n$; O_0^0 shifts all terms equally and is not relevant; terms with odd n disappear due to time reversal symmetry). μ_{B} is the Bohr magneton, $\boldsymbol{B}$ the magnetic field, and the principal values of the **g** tensor and the hyperfine coupling tensor **A** have to be derived from the spectra in zircons and scheelites. For Tb^{4+}, the second term appears so strong that the Zeeman term is no longer very much larger. $S = 7/2$ and $I = 3/2$ was inserted.

3. Results

3.1 $ZrSiO_4 : Tb^{4+}$

Representative spectra and rotational diagrams for this compound were already shown in the last section. In Fig. 1, apart from several single lines, five quartets, and Fig. 2 two quartets can be identified as to be expected for the EPR of Tb^{4+} with hyperfine structure ($I = 3/2$). The spectra as a whole indicate that the zero field splitting is so large relative to the Zeeman splitting that the strong field approximation is no longer valid. The rotational diagrams of Fig. 3 reveal axially symmetric spectra belonging to tetravalent terbium at the four equivalent (crystallographically and magnetically) zirconium sites of the lattice. The system can therefore be described completely by rotations about two axes, where the crystallographic c axis coincides with the magnetic z axis.

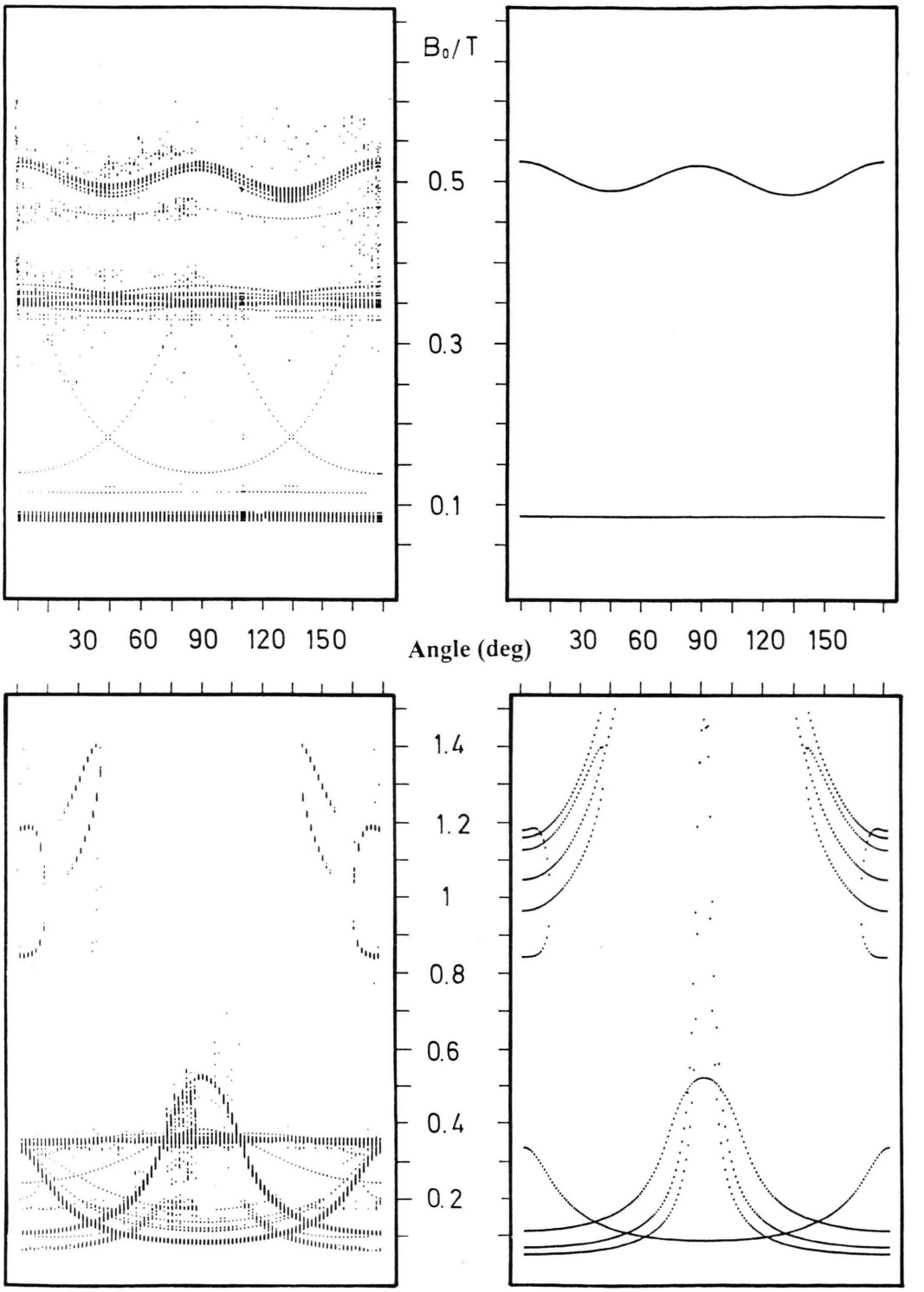

Fig. 3. Measured (left) and simulated rotational diagrams (right) for Tb^{4+} in $ZrSiO_4$:Tb^{4+} at 9.379 GHz and 77 K. The diagrams at the top belong to a rotation about the c axis, those at the bottom to a rotation about $a \perp c$. In all simulated rotational diagrams the hyperfine interaction is omitted to get a clear look of the zero field splitting.

Table 1. Spin Hamiltonian parameters of Tb^{4+} in various zircon and scheelite structure silicates and germanates in tetragonal symmetry as determined within the frame of this work. Hyperfine structure was only resolved in exceptional cases.

	T/K	$g_{\parallel}$	$g_{\perp}$	B_2^0/h GHz	B_4^0/h GHz	B_4^4/h GHz	$A_{\parallel}/h$ MHz	$A_{\perp}/h$ MHz
$ZrSiO_4$	293	1.999(2)	1.989(2)	9.667(5)	0.0048(8)	0.0108(8)	±94.2(9)	±99.8(9)
	77	1.999(2)	1.995(2)	9.984(5)	0.0046(8)	0.0111(8)	±94.7(9)	±101.2(9)
	50	1.998(2)	1.994(2)	10.022(5)	0.0049(8)	0.0104(8)	±94.7(9)	±101.2(9)
$HfSiO_4$	293	2.000(2)	1.992(2)	10.390(5)	0.0039(8)	0.0073(8)		
	77	2.001(2)	2.001(2)	10.784(5)	0.0047(8)	0.0074(8)		
$ThSiO_4$	293	2.011(5)	1.998(5)	5.688(6)	0.0014(9)	0.0159(9)		
	77	2.009(5)	2.000(5)	6.091(6)	0.0013(9)	0.0210(9)	±98.1(1.2)	
$ThGeO_4$	293	1.997(5)	1.997(5)	8.677(9)	−0.0104(89)	0.0212(18)		
	77	1.997(5)	1.985(5)	9.030(9)	−0.0109(89)	0.0228(18)		±91.7(1.2)
$ZrGeO_4$	293	1.998(2)	1.998(2)	10.778(5)	0.0062(8)	0.0207(8)		
	77	2.002(2)	2.002(2)	11.230(5)	0.0091(8)	0.0205(8)		
	50	2.002(2)	2.002(2)	11.362(5)	0.0092(8)	0.0196(8)		98.1(1.1)
$HfGeO_4$	293	2.000(2)	2.000(2)	10.299(5)	0.0062(8)	0.0206(8)		
	77	2.000(2)	2.000(2)	10.595(5)	0.0078(8)	0.0215(8)		

From the rotational diagrams and their simulations the positions of the crystal axes in the field were determined (misorientation), as well as the principal values of the **g** tensor and the ZFS parameters.

The principal **A** values were already extracted from the spectra of Figures 1 and 2. It was possible to assign all the lines arising from Tb^{4+} exactly to the various transitions of the spin Hamiltonian (1). The EPR parameters determined within the frame of this procedure in detail are listed in Table 1 together with the other results. Additional lines, especially observable at low temperatures, were found to belong to Gd^{3+} impurities. Measurements were also made at 293 K and 50 K. The character of the tetragonal spectrum remains the same, but several parameters appear to be temperature dependent. By comparing the intensity of certain transitions at various temperatures the sign of the ZFS parameters B_2^0, B_4^0 and B_4^4 could be determined to be positive.

Using a smaller crystal, the same type of measurements and simulations was carried out at Q band frequencies (not shown). Within the limits of accuracy the parameters finally obtained were exactly the same as those from the X band spectra. Finally, powder patterns of Tb^{4+} were analyzed. Without knowledge of the single crystal spectra their lines cannot be assigned unequivocally, or in other words, it is not possible to obtain an estimate of the ZFS parameters from solely a powder pattern. This is due to the large zero field splittings which require single crystal data.

3.2 $HfSiO_4$: Tb^{4+}

Because of the small crystal size available, only Q band measurements could be performed. Spectra and rotational diagrams are shown in Figures 4 and 5. Compared with the EPR spectra of the last section the number of lines is greatly reduced, first because the

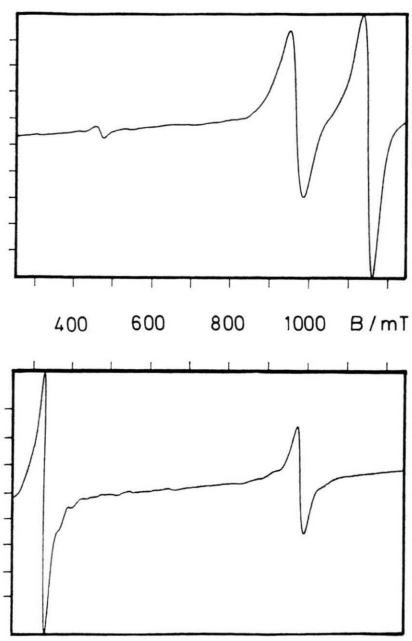

Fig. 4. EPR spectra of Tb^{4+} in $HfSiO_4$:Tb^{4+} with $B_0 \parallel c$ (top) and $B_0 \perp c$ (bottom) measured at 33.88 GHz and 293 K.

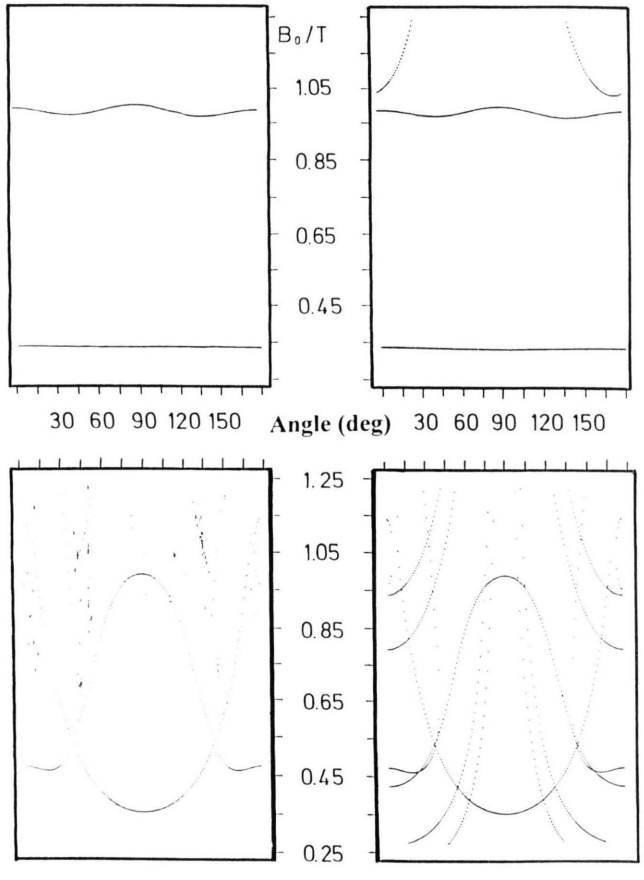

Fig. 5. Measured (left) and simulated rotational diagrams (right) for Tb^{4+} in $HfSiO_4$:Tb^{4+} at 33.88 GHz and 293 K. Top: rotation about the *c* axis; bottom: rotation about the *a* axis.

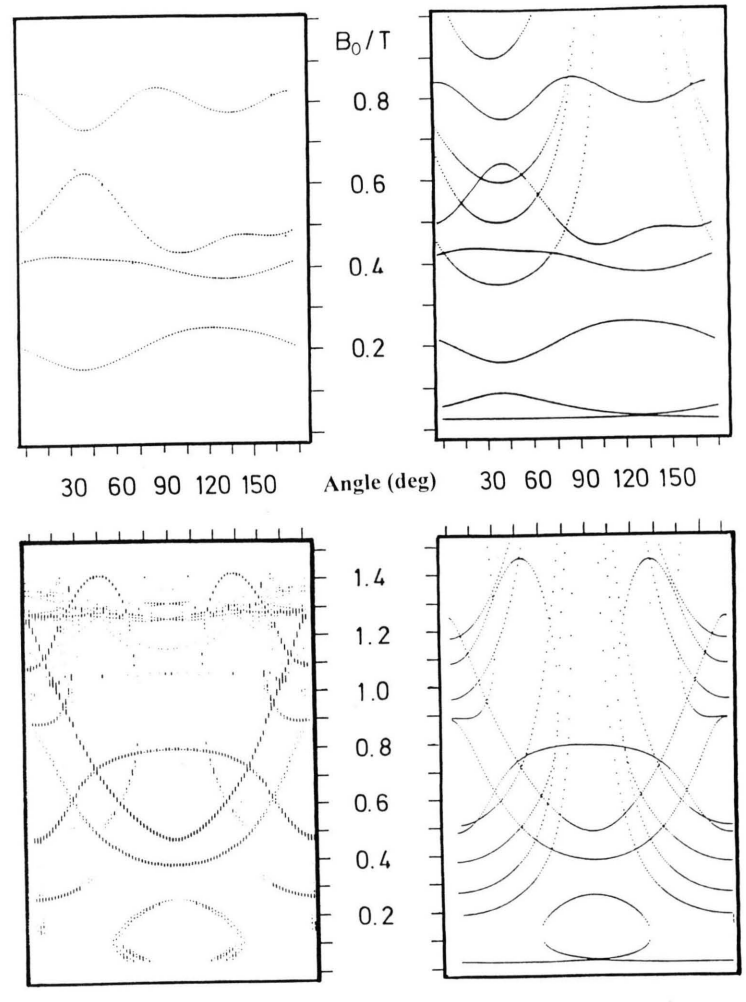

Fig. 6. Same as Fig. 5, but for $ThSiO_4$:Tb^{4+} at 77 K.

quality of the crystal was worse and the hyperfine structure is not resolved; secondly only signals originating from Tb^{4+} exist. The EPR parameters of Table 1 were derived in the same way as described in the last sections.

3.3 $ThSiO_4:Tb^{4+}$ and $ThGeO_4:Tb^{4+}$

Thorium silicate and germanate doped with terbium are both colourless and do not give EPR signals. The reason that terbium is here introduced in form of Tb^{3+} is probably the similar ionic radius of Th^{4+} and Tb^{3+}. After X irradiation with a K_α source for five days the terbium was oxidized and could be identified as Tb^{4+}. In $ThSiO_4:Tb^{4+}$ more lines of the Tb^{4+} spectrum could be identified than in $HfSiO_4$, cf. Figure 6. Additional signals recognizable at high fields arise probably from colour centres of the type of SiO_4^{5-}.

For $ThGeO_4:Tb^{4+}$ less lines originating from Tb^{4+} were observed (not shown, spectra similar to those of $HfSiO_4:Tb^{4+}$) since the EPR was dominated by signals from colour centres. It was however possible, as in the case of $ThSiO_4:Tb^{4+}$, to determine the ZFS parameters, cf. Table 1.

3.4 Crystals with Scheelite Structure

$ZrGeO_4:Tb^{4+}$ crystals are red and $HfGeO_4:Tb^{4+}$ crystals orange coloured. Terbium is tetravalent already without irradiation, and all observed EPR signals arise from Tb^{4+}. The lines are inhomogeneously broadened and no hyperfine structure can be resolved. Most information was again obtained from the rotational diagrams, especially from the EPR spectra at the rotation about an axis perpendicular to c, cf. Figure 7. As in the case of the crystals with zircon structure, tetragonal spectra were found. The EPR parameters are again listed in Table 1.

4. Discussion and Conclusions

4.1 EPR Spectra and Parameters

In all the hosts, the EPR spectra of Tb^{4+} look much more complex than those of other S-state ions, because the zero field splitting is extremely large. The crystal field term is no longer smaller than the Zeeman interaction, and the procedure of line assignment and correspondingly the data evaluation has to be more

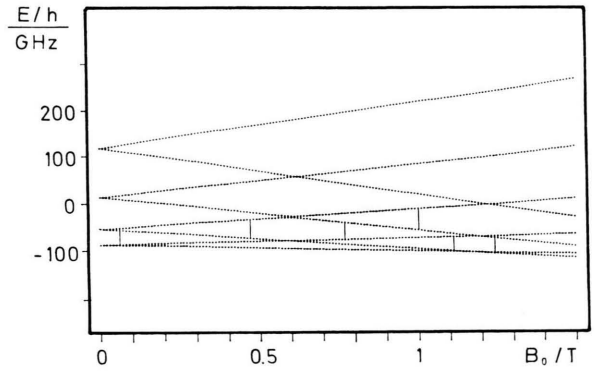

Fig. 8. Energy level diagram of Tb^{4+} in $ThSiO_4:Tb^{4+}$ with $B_0 \| z$ at 293 K. EPR transitions observed at 33.95 GHz are indicated.

sophisticated. The hyperfine coupling constants are also larger. Since strong field approximation and perturbation treatment cannot be applied, $m_s = \pm 7/2$, $\pm 5/2$, $\pm 3/2$ and $\pm 1/2$ are no longer good magnetic quantum numbers to describe the transitions, and the intensities behave unusual.

An example of the energy levels and the observed transitions is shown in Fig. 8 for Tb^{4+} in the crystal with the smallest zero field splitting. The diagram was constructed from the data. One recognizes the splitting of the $^8S_{7/2}$ ground state in the large axial crystalline field into four doublets. For intensity reasons, transitions between the highest levels could not be observed, but selection rules like $\Delta m_s = \pm 1$ were not obeyed.

Nevertheless, all the spectra and their rotational dependences could be fit with high accuracy to the spin Hamiltonian (1). They appear to be axially symmetric and exclusively characteristic of Tb^{4+} in tetragonal sites, i.e., the relevant ZFS parameters are B_2^0, B_4^0 and B_4^4. B_2^2 is zero (axial symmetry) and the B_6^m were found to be extremely small (0 ± 5 MHz). The numerical results for the four crystals with zircon structure and the two with scheelite structure are summarized in Table 1 together with the other EPR parameters. The principal values of the **g** tensor deviate very little from $g = 2.0023$ for the free electron. Hyperfine coupling will be discussed further below in comparison with Gd^{3+}.

The ZFS parameters are clearly temperature dependent. The dominant crystal field parameter B_2^0 decreases about linearly with temperature; the succession from $ZrGeO_4$ with the largest B_2^0 via $HfSiO_4$,

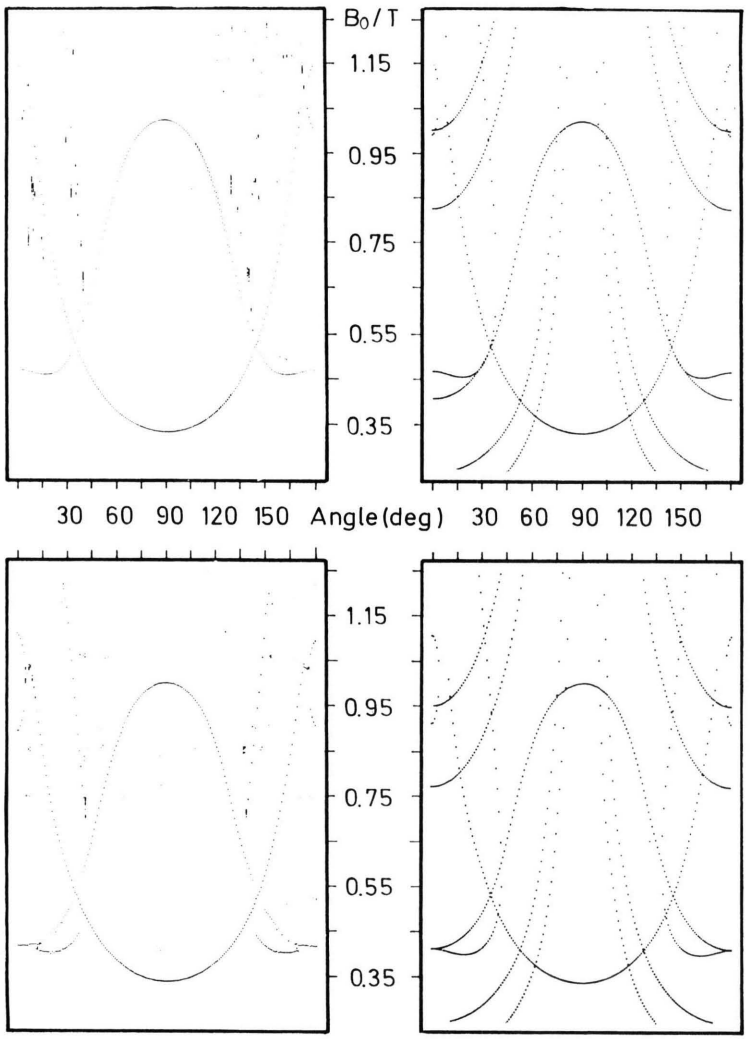

Fig. 7. Measured (left) and simulated rotational diagrams (right) for Tb^{4+} in $ZrGeO_4$:Tb^{4+} (top) and $HfGeO_4$:Tb^{4+} (bottom). Only the rotations about the *a* axis are shown. The data were recorded at Q band frequencies and room temperature (293 K).

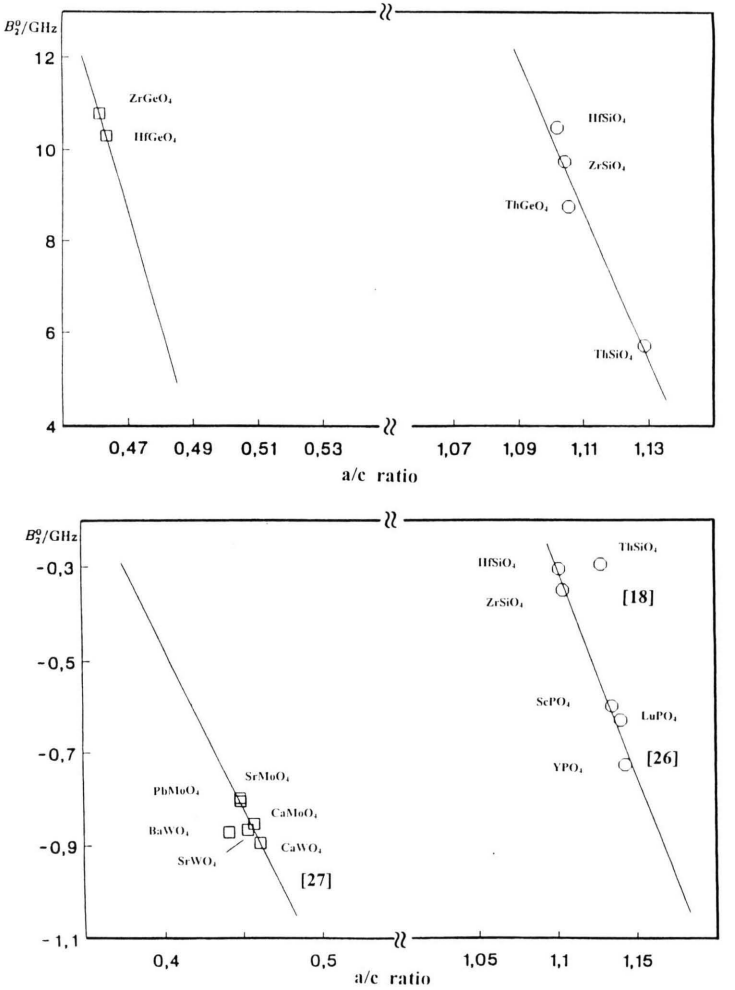

Fig. 9. Top: ZFS parameter B_2^0 at 293 K for Tb^{4+} in scheelite (left) and zircon structure (right) germanates and silicates as a function of the lattice constant ratio. Bottom: same presentation for Gd^{3+} in various crystals; these data are taken from the literature as indicated.

$HfGeO_4$, $ZrSiO_4$, $ThGeO_4$ to $ThSiO_4$ with the smallest value remains unaffected.

4.2 Incorporation of Tetravalent Terbium

The assignment of the spectra to tetravalent terbium in tetragonal sites is unequivocal although no $\pm 7/2$ transitions were observed. Divalent terbium with $S = 5/2$ is chemically not stable, and its ionic radius is much too large. A further argument against Tb^{2+} are our observed principal g values. We have also studied the UV spectra and concluded that the colour is determined in all host crystals by the $4f \rightarrow 5d$ transition of Tb^{4+}.

The tetragonal spectra can be assigned to Tb^{4+} ions substituted at the sites of Zr, Hf, and Th. Silicon and germanium can be eliminated as sites for rare earth substitution, since their ionic radii are considerably smaller. Zr^{4+} and Hf^{4+}, however, do not only carry the same charge, but possess a rather similar ionic radius. Only the ionic radius of Th^{4+} is about 20% larger, and X-ray irradiation has to be applied to incorporate terbium as Tb^{4+} in $ThSiO_4$ and $ThGeO_4$.

The local environment in the six host crystals must have the same symmetry, and only the magnitude of the crystal field splitting is different. This holds as well for Tb^{4+} doped crystals with scheelite structure, which – as far as we are aware – have not yet been studied by EPR. It is difficult to compare the results with those of other authors who examined Tb^{4+} in sites with different symmetry. Comparison with the early work on Tb^{4+} in zircon [1] show that only the hyperfine coupling and the order of magnitude of the zero field splitting could be correctly determined at that time. The interpretation of a second study [2] is no longer valid. For obtaining the correct ZFS data, because of the complex spectra, it is really necessary to measure the angular dependences in detail.

4.3 Comparison with Gd^{3+} in Zircon Structure Silicates

We have also measured the EPR spectra of Gd^{3+} in $ZrSiO_4$:Gd^{3+} (not shown). Within the limits of accuracy, our observed parameters agree with those of previous studies [18, 19]. Such data are available in addition for $HfSiO_4$:Gd^{3+} and $ThSiO_4$:Gd^{3+} [18]. In contrast to our EPR spectra of Tb^{4+} in zircon structure silicates, Gd^{3+} spectra were observed which exhibited both tetragonal and orthorhombic symmetry [19]. The ZFS parameters are much smaller, and the observed spectra were simpler to analyze. Table 2 shows that the dominating splitting parameter for the tetragonal sites is 20 to 30 times larger for Tb^{4+} than that for Gd^{3+}. The absolute value of B_2^0 decreases in both cases at elevated temperatures, but since it is negative for Gd^{3+}, B_2^0 increases there. The same tendency holds if the relationship of B_0^2 with the ionic radii of Si, Hf and Th, whose sites the rare earth ions occupy, is considered; the absolute values of B_0^2 decrease with the effective metal radius.

Table 2. Ratio of the ZFS parameters of Tb^{4+} and Gd^{3+} in tetragonal sites of three silicates with zircon structure. The data of Gd^{3+} are taken from [18].

		$B_2^0(Tb^{4+})/B_2^0(Gd^{3+})$	$B_4^0(Tb^{4+})/B_4^0(Gd^{3+})$	$B_4^4(Tb^{4+})/B_4^4(Gd^{3+})$
$ZrSiO_4$	293 K	−27.4	3.4	−12.6
	77 K	−25.1	3.3	−11.5
$HfSiO_4$	293 K	−33.8	2.3	−8.5
	77 K	−30.5	2.3	−9.8
$ThSiO_4$	293 K	−19.2	10.5	−4.1
	77 K	−19.6	14.2	−3.7

Comparison of hyperfine structure data (^{155}Gd, ^{157}Gd [18]; ^{159}Tb, this work) shows that the calculated atomic s character in the molecular orbital is in all three cases about 0.7%. This follows from the mean Hfs parameters measured (13, 17 and 98 MHz) and the values for 100% s character (−1947, −2546, and 13630 MHz, [20]).

4.4 Zero Field Splitting

The most remarkable result is the extremely large crystal field splitting of Tb^{4+} in the tetragonal sites, not only if compared with other S-state ions. From simple considerations of the ligand field strengths and ionic charges, only about twice the ZFS of Gd^{3+} had been expected. At first sight, a possible explanation could be the nearby excitation of a $4f^6 5d^1$ state which is responsible for the colour. For Tb^{4+} in zircon we measured an excitation energy of 3.44 eV, which is smaller than that of 9.9 eV known for Gd^{3+} (colourless) [21]. A spin-orbit admixture of such a state or other excited states into the $^8S_{7/2}$ ground state would, however, change the principal g values away from those of the free electron, and this not at all observed. Therefore, excited $4f^7$ states, such as $^6P_{7/2}$ with an even larger excitation energy (free ion: 5.57 eV [22]), can also be ruled out.

Several attempts have been made to calculate the zero field splittings of S-state ions in crystals either from first principles or semiempirically from nearest neighbour contributions. Most successful in explaining ZFS parameters from the local structure of S-state ions in a variety of crystals was the Newman superposition model [23–25]. This model provides a method of analysing the observed splittings by adding up the contributions of single ligands as function of their distance. As suggested by Newman et al., the ZFS data can be explained by "intrinsic parameters" $\bar{b}_n^m(R_0)$ taken at a mean distance R_0 which is connected with the observable B_n^m via effective coordination factors. The dependence of $\bar{b}_n^m$ on the local structure can be approximated by a power law whose exponent has to be determined experimentally.

Application of the superposition model to Tb^{4+} in zircon and scheelite structure silicates and germanates fails to explain the EPR results, at least if the model is used in its original form. It is, however, possible to obtain reasonable $\bar{b}_n^m$ values, but for the relation with geometrical parameters laws different from those suggested by Newman had to be assumed. Compared with Gd^{3+}, $\bar{b}_n^m$ turns out be about ten times larger. The size of the ZFS as induced by the ligand field is much more determined by the paramagnetic ion itself rather than by the environment. The dependence on the various crystals can be correctly explained.

In this context it is worth mentioning that for both Tb^{4+} and Gd^{3+} in zircon and scheelite structures, the dominating parameter B_2^0 appears to be a linear function of the lattice constant ratio a/c. Figure 9 shows this relationship; for comparison, corresponding linear dependences are shown for the known zero field splittings of Gd^{3+} in zircons [18, 26] and scheelites [27]. The lattice constants were available in the literature (zircon structure silicates [28–30], germanates [31] and phosphates [32], scheelite structure germanates [31, 33], molybdates [34, 35] and tungstates [35, 36]).

The authors are grateful to the Deutsche Forschungsgemeinschaft (DFG) for supporting this work.

This paper is dedicated to the memory of Professor Dr. G. Lehmann, who established the EPR spectroscopy of crystals in Münster and initiated this research before his death in 1990.

[1] D. R. Hutton and R. J. Milne, J. Phys. C. **2,** 2297 (1969).
[2] L. V. Bershov, Geokhimiya **1,** 48 (1971).
[3] J. M. Baker, J. R. Chadwick, G. Garton, and J. P. Hurell, Proc. Roy. Soc. London A **286,** 352 (1965).
[4] C. B. Azzoni, G. L. Del Nero, G. Lanzi, and M. Cola, Rend. 1st. Lomb. Sci. Lett. A **105,** 974 (1971).
[5] Y. S. Greznev, M. M. Zarpipov, and V. G. Stepanov, Sov. Phys.-Solid State **7,** 2937 (1966).
[6] C. B. Azzoni, G. L. Del Nero, G. Lanzi, and M. Cola, Rend. 1st. Lomb. Sci. Lett. A **107,** 312 (1973).
[7] L. S. Kornienko and A. O. Rybaltovskii, Sov. Phys.-Solid State **13,** 1609 (1972).
[8] R. Aldous and J. M. Baker, J. Phys. C **10,** 4837 (1977).
[9] Y. Husatsu, J. Solid State Chem. **100,** 136 (1992).
[10] N. Guskos, S. M. Paraskevas, A. Koufoudakis, C. Mitros, H. Gamari-Seale, V. Psykaris, D. Niarchos, J. Kuriata, and I. Kruk, Exp. Tech. Phys. **39,** 555 (1991).
[11] Ying Wu and Chunshan Ihi, Solid State Commun. **95,** 319 (1995).
[12] P. E. Fielding, Aust. J. Chem. **23,** 1513 (1970).
[13] B. M. Wanklyn, J. Crystal. Growth **37,** 51 (1977).
[14] T. Behner, Thesis (1991) and T. Böttjer, Thesis (1991), unpublished.
[15] S. Remme, Thesis (1985); F. Prissok, Thesis (1989).
[16] A. Abragam and B. Bleaney, Electron Paramagnetic Resonance of Transition Ions, Clarendon Press, Oxford 1970.
[17] K. W. H. Stevens, Proc. Phys. Soc. London A **65,** 209 (1952).
[18] M. M. Abraham, G. W. Clark, C. B. Finch, R. W. Reynolds, and H. Zeldes, J. Chem. Phys. **50,** 2057 (1969).
[19] R. W. Reynolds, L. A. Boatner, C. B. Finch, A. Chatelain, and M. M. Abraham, J. Chem. Phys. **56,** 5607 (1972).
[20] J. R. Morton and W. F. Preston, J. Magn. Reson. **30,** 577 (1978).
[21] A. S. Marfunin: Spectroscopy, Luminescence and Radiation Centers in Minerals, Springer-Verlag, Berlin 1979.
[22] S. Fraga, J. Karwowski, and K. M. S. Saxena, Handbook of Atomic Data, Elsevier Publ. Comp., Amsterdam 1976.
[23] D. J. Newman, Adv. Phys. **20,** 197 (1971).
[24] D. J. Newman and W. Urban, Adv. Phys. **24,** 793 (1975).
[25] D. J. Newman and B. Ng, Rep. Prog. Phys. **52,** 699 (1989).
[26] M. Rappaz, M. M. Abraham, J. O. Ramey, and L. A. Boatner, Phys. Rev. B **23,** 1012 (1981).
[27] Vishwamittar and S. P. Puri, J. Chem. Phys. **61,** 3720 (1974).
[28] R. M. Hazen and L. W. Finger, Amer. Mineral. **64,** 196 (1979).
[29] J. A. Speer and B. J. Cooper, Amer. Mineral. **67,** 804 (1982).
[30] M. Taylor and R. C. Ewing, Acta Crystallogr. B **34,** 1074 (1978).
[31] A. Ennaciri, A. Kahn, and D. Michel, J. Less-Commion Met. **124,** 105 (1986).
[32] W. O. Milligan, D. F. Mullica, G. W. Beal, and L. A. Boatner, Inorg. Chim. Acta **60,** 39 (1982).
[33] A. Ennaciri, D. Michel, M. Perez y Jorba, and J. Pannetier, Mat. Res. Bull. **19,** 793 (1984).
[34] J. Leciejewicz, Z. Krist. **121,** 158 (1965).
[35] E. Gürmen, E. Daniels, and J. S. King, J. Chem. Phys. **55,** 1093 (1971).
[36] A. Zalkin and D. H. Templeton, J. Chem. Phys. **40,** 501 (1964).